RESEARCH

Stability analysis and control technology of gob-side entry retaining with double roadways by filling with high-water material in gently inclined coal seam

Shengrong Xie[1,2] · En Wang[1,3] · Dongdong Chen[1,2] · Hui Li[1] · Zaisheng Jiang[1] · Hongzeng Yang[4]

Abstract

To ameliorate the defects of insufficient support resistance of traditional roadside filling bodies for gob-side entry retaining (GER), overcome the inability to adapt to the deformation of surrounding rock, and isolate the goaf effectively, a new type of high-water material as a roadside filling body for GER technology with double roadways was proposed. The instability analysis and control technology of GER with double roadways by filling high-water material into a gently inclined coal seam were studied. The basic mechanical properties of the new high-water material were investigated through laboratory experiments, and their main advantages were identified. The reasonable width of the roadside filling wall of a high-water material was obtained by combining ground pressure observation and theoretical calculations. The distribution characteristics of the stress and plastic zone of surrounding rock of GER after being stabilized by the disturbance of the working face were studied using numerical simulations, and the failure range of GER by filling with high-water material was revealed. Based on this, a coupling control technology of anchor cables and bolts + single props + metal mesh + anchor bolts is proposed. Through the coupling methods of arranging borehole peeping and observing the convergences of surrounding rock, the results demonstrate that GER with double roadways by filling with a 1.8-m-wide high-water material has a good control effect. The above research will play an active role in promoting the application of high-water materials in GER roadside filling.

Keywords High-water material · Gob-side entry retaining with double roadways · Stability analysis · Gently inclined coal seam · Control technology

1 Introduction

Gob-side entry retaining (GER) with no pillars has many advantages, such as improving the coal recovery rate, realizing Y-shaped ventilation, easing mining and excavation replacement, and reducing excavation cost, and has been widely used in all types of coal mines in China (Bai et al. 2015; Chen et al. 2020; Feng and Zhang 2015; He et al. 2017; Kong et al. 2021; Meng et al. 2021). Traditional GER roadside supports have mainly employed low-strength support methods such as wooden stacks, gangue belts, dense pillars, and concrete blocks (Bai et al. 2004; Huang et al. 2011; Yang et al. 2016). However, because of the shortcomings of traditional roadside supports, such as resistance and shrinkage and their inability to adapt to the large deformation of the surrounding rock and to effectively isolate the goaf, their use has been gradually eliminated. New high-water materials offer several advantages (Batugin et al. 2021; Chang et al. 2021; Orsborn and Zantos 1988; Tomlinson and Caroline 1990; Quesada-Kimzey et al. 2016; Li and Liu 2018; Park et al. 2019; Wang et al. 2021; Wu et al. 2020; Zhou et al. 2020): They exhibit obvious plastic characteristics, undergo quick solidification, provide a rapid increase in resistance, have high strength, offer quick support of the roof, produce a

✉ Dongdong Chen
chendongbcg@163.com

1 School of Energy and Mining Engineering, China University of Mining and Technology-Beijing, Beijing 100083, China

2 Beijing Key Laboratory for Precise Mining of Intergrown Energy and Resources, China University of Mining and Technology-Beijing, Beijing 100083, China

3 Department of Civil Engineering, University of British Columbia, Vancouver, BC V6T 1Z4, Canada

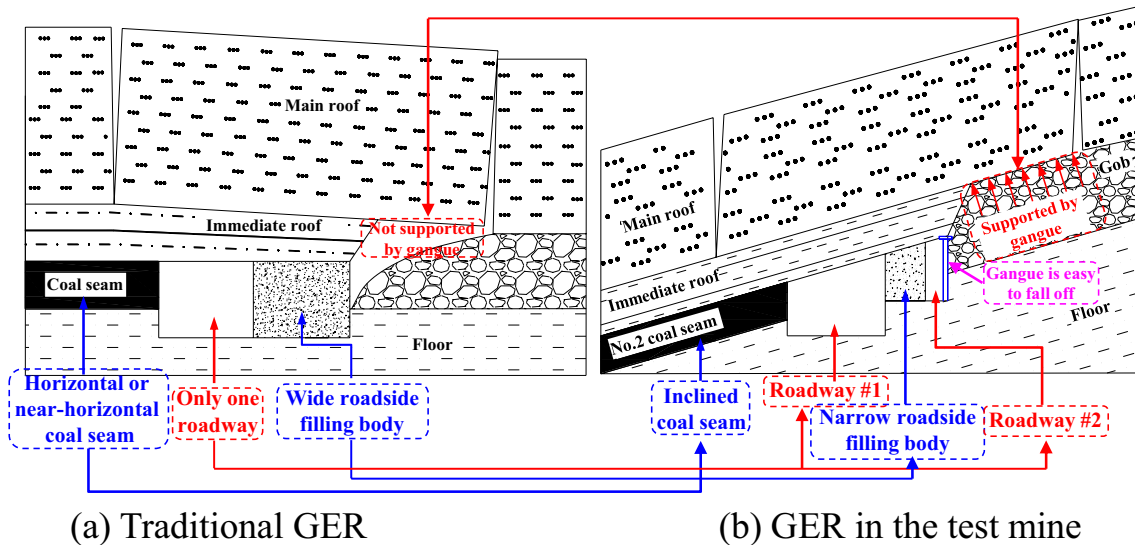4 Hebei Coal Science Research Institute Corporation Ltd., Xingtai 054000, China

Fig. 1 Comparison between traditional GER and GER with double roadways in the test mine

specific compression rate after curing, are low cost, and are adaptable to the large deformation of surrounding rock of GER. Therefore, studying the engineering application of high-water material in GER roadside filling is essential for safe mining, improving coal recovery rate, and increasing economic benefits.

In traditional GER roadside supports, dense pillars are rarely used because of the problems of large supporting workload and poor supporting and isolation effects of the goaf (Chen et al. 2021a; Zhang et al. 2020). The gangue stacking method (He et al. 2017) can easily cause excessive roof sinking and result in poor stability, making it difficult to adapt and to promote and apply. Prefabricated block masonry wall (Kang et al. 2010) can form high-strength walls for isolating the goaf, but they still cannot solve the problem of the connection between the wall and the roof. Because they cannot be reliably sealed, their effect is poor. Concrete wall (Tang et al. 2010) have wide adaptability and high bearing capacity and offer improved safety and reliability. However, the filling cost is high, the construction is complicated, and the speed of increase in strength cannot meet the high-yield, high-efficiency needs of the working face, and there is also a problem of slurry leakage. Although concrete paste filling technology (Huang et al. 2015) can be applied in situ and in an environmentally friendly manner, its wide promotion poses challenges because of the construction process and paste strength. Therefore, the above-mentioned roadside supports have the disadvantages of supporting resistance, and shrinkage cannot adapt to the large deformation of surrounding rock of GER nor effectively isolate the goaf, making it difficult to achieve high mechanization. Consequently, it is necessary to study new filling materials with suitable strength, shrinkage pressure and timely closure of the goaf.

The new high-water material for roadside filling of GER has the characteristics of early strength, quick solidification, small volume strain, incompressibility under the action of a three-dimensional force, and an obvious plastic characteristic. Compared with traditional GER, 2202 GER in the test mine has the following features as shown in Fig. 1: (1) a gently inclined coal seam, (2) a roadside filling body comprising a 1.8-m-wide high-water material, (3) GER with a double roadway, and (4) ease of entry of the gangue in the goaf behind the working face into the outer roadway of GER. In view of the above characteristics of this high-water material, as well as considering that the majority of existing research results on GER focus on a single retained roadway in a nearly horizontal coal seam, in this project we study a GER structure with double roadways by filling with high-water material in a gently inclined coal seam in the test mine, China. The basic mechanical properties of high-water materials were analyzed through laboratory tests. Based on the construction of a mechanical model of GER with double roadways by filling with high-water material in a gently inclined coal seam, the reasonable width of roadside high-water material of the GER structure was determined. FLAC3D numerical simulations were used to study the distribution characteristics of the vertical stress and plastic zone of surrounding rock when the headgate is not disturbed and is affected stably by the mining of working face 2202. The failure range of surrounding rock of GER was revealed. A coupling control technology, consisting of anchor cables and bolts in the roof and solid coal and single props in the entry-in support and goaf side of the outer roadway with anchor bolts in roadside high-water material and short anchor cables below the filling body, is proposed and industrial tests were conducted. Through the methods of arranging borehole
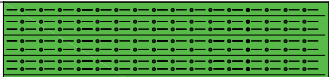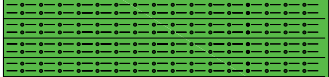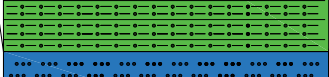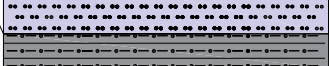
Rock stratum	Legend of rock column	Thickness /m	Lithology description
Sandy mudstone		12.95	Dark gray, layered, evenly jointed, rich in plant fossil fragments, brittle and semi-hard, flat section
Fine-grained sandstone		6.02	Deep gray, layered, fissure developed, containing plant rhizome fossils
Carbonaceous mudstone		1.95	Argillaceous structure, angular fracture, local interbedding with siltstone, undeveloped bedding
No.2 coal seam		**1.62**	Black, massive, vitrinite-dominated, heterogeneous fracture, endogenous and exogenous fracture
Mudstone		3.05	Gray, flat fracture, horizontal and gentle wave bedding, siliceous cementation
Siltstone		4.50	Light gray and dark gray, medium thick layered, horizontal bedding and wavy texture
Mudstone		2.04	Gray, flat fracture, horizontal and gentle wave bedding, siliceous cementation

Fig. 2 Coal and rock strata histogram

peeping, observing the convergences of surrounding rock, and measuring the load in the filling body, the control effects of surrounding rock of GER were systematically analyzed. The research results can play an active role in promoting the application of high-water materials in GER roadside filling in coal mines.

2 Engineering geology

2.1 Geological overview of the working face

The test mine is located in southwestern Jinzhong County, Shanxi Province, China. Mainly mined is the No. 2 coal seam with an average buried depth of approx. 670 m. 2202 working face is located south of the No. 2 coal mining area with an F_2 fault protective coal pillar in the south. The surface of 2202 working face is located at Fanwang Village, the eastern part of which belongs to the hills and valleys and has good drainage. The dip angle of the No. 2 coal seam is 14°–23°, with an average dip angle of 16°, and it belongs to a gently inclined coal seam. The average thickness of the coal seam is 1.62 m and its consistent coefficient f is 2–3 with the bedding and joints relatively developed. The upper part of the coal seam is a pseudo-roof mudstone of 0–0.2 m; the immediate roof is carbonaceous mudstone of 1.95 m, and the main roof is fine-grained sandstone of 6.02 m. A comprehensive histogram of the coal and rock strata is shown in Fig. 2.

The inclination length of 2202 working face is 180 m, and the tendency length is 1300 m. The mining method for 2202 working face is strike longwall comprehensive mechanized mining. The headgate of 2202 working face is excavated along the roof of the No. 2 coal seam, which is reserved by the method of GER by filling with the new high-water material for the next working face with a net cross section of 4.2 m × 2.9 m (width × middle height).

2.2 Support scheme for headgate

The roof bolts for 2202 headgate are Φ20 mm × 2000 mm threaded steel resin bolts whose anchorage capacity is ≥ 70 kN and pre-tightening torque is ≥ 150 N m with a row and line spacing of 800 mm × 800 mm. The bolts on the two sides of the headgate are Φ16 mm × 2000 mm threaded steel resin bolts whose anchorage capacity is ≥ 50 kN and pre-tightening torque is ≥ 120 N m with a row and line spacing of 800 mm × 800 mm. The anchor cables on both sides and the roof are Φ17.8 mm × 6000 mm steel strands with a pre-tightening force of ≥ 125 kN and a 300 mm × 300 mm × 20 mm square pallet. Two anchor cables are arranged in the middle roof with a spacing of 1600 mm × 1600 mm. The anchor cables on the right side of the headgate are arranged with a row and line spacing of 1600 mm. The headgate support at 2202 working face is shown in Fig. 3.
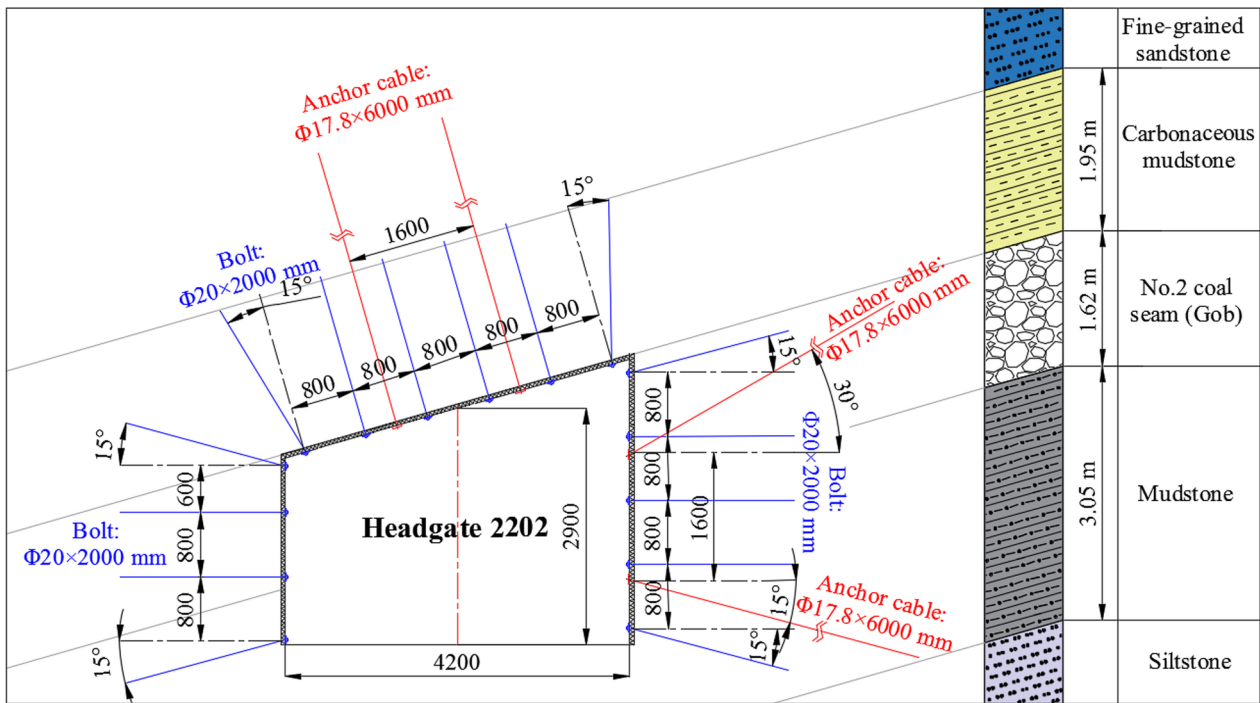
Fig. 3 Suppor diagram of the headgate

3 Basic properties of roadside high-water material

To ascertain the basic mechanical properties of roadside high-water material in GER of working face 2202 in the test mine, multiple laboratory tests are conducted to study the main composition, micromorphology, stress–strain relationship, and the connection among elastic modulus, peak stress, and curing ages. These tests provide a theoretical basis for the application of high-water materials in GER roadside filling.

3.1 Basic composition and micromorphology

The high-water material (Xia et al. 2018) is a new hydraulic material composed of two main materials, A and B, two auxiliary materials, AA and BB, and water. The X-ray diffraction pattern of the high-water material (Fig. 4) and the main
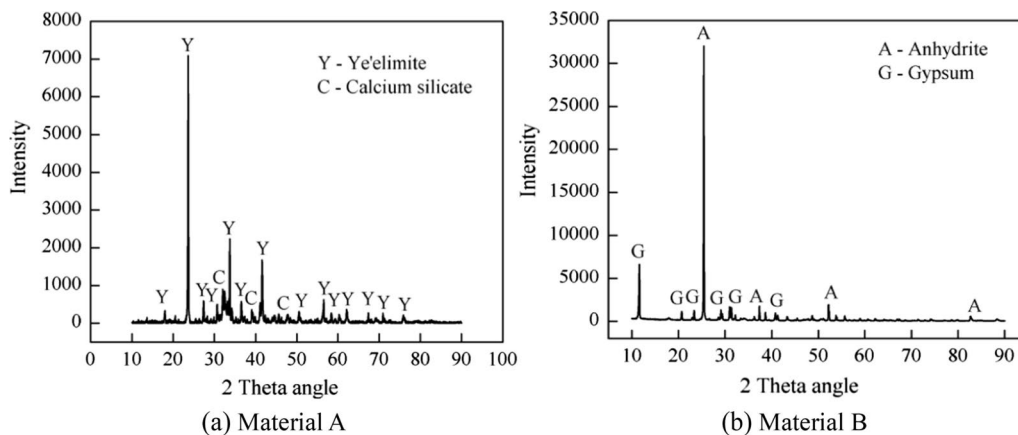

(a) Material A   (b) Material B

Fig. 4 X-ray diffraction pattern of high-water material

Material	Yeelimite	Calcium silicate	Anhydrite	Gypsum
A	68.15	31.85	0	0
B	0	0	74.85	25.15

ingredients of A and B (Table 1) are obtained by laboratory tests. It can be seen that the main components of material A are sulpho-aluminate cement and calcium silicate, while B is mainly composed of anhydrite and quicklime. Materials AA and BB are auxiliary materials of A and B, respectively; they are composite accelerators composed of an accelerator and a suspension dispersant, respectively.

Configuring the high-water material entails mixing materials A and AA and materials B and BB with water to make slurries A and B, respectively, through the preparation system. Water is added to AA and BB materials to make the slurries active and then added to the preparation of slurries A and B. The slurries of high-water materials A and B are used together at a ratio of 1:1. The water-to-cement ratio of high-water material in GER roadside

filling in the test mine is 1.6:1. After the two slurries are fully mixed, they quickly set and harden. They are then processed to form standard specimens of high-water material with a certain strength, as shown in Fig. 5.

The micromorphology obtained by a laboratory computed tomography scanner of the high-water material after curing for 28 days with a water-to-cement ratio of 1.6:1 is shown in Fig. 6. The hydration product of the high-water material is found to be mainly ettringite (with a molecular formula of $3CaO \cdot Al_2O_3 \cdot 3CaSO_4 \cdot 32H_2O$), and its microscopic morphology is mostly slender needle-like crystals with small crystal diameters. Its stone body is mainly composed of a fine branch net structure, and each branch and column is overlapped and staggered with a disordered arrangement. The distance between the branches and columns is obvious, and the gap is large. The massive structure is calcium carbonate, and its distribution is relatively concentrated, part of which forms a specific overall structure. Micropores are developed in the surface microstructure. The branches and columns of the stone body are relatively compact because of the low water content of roadside high-water material in the test mine.
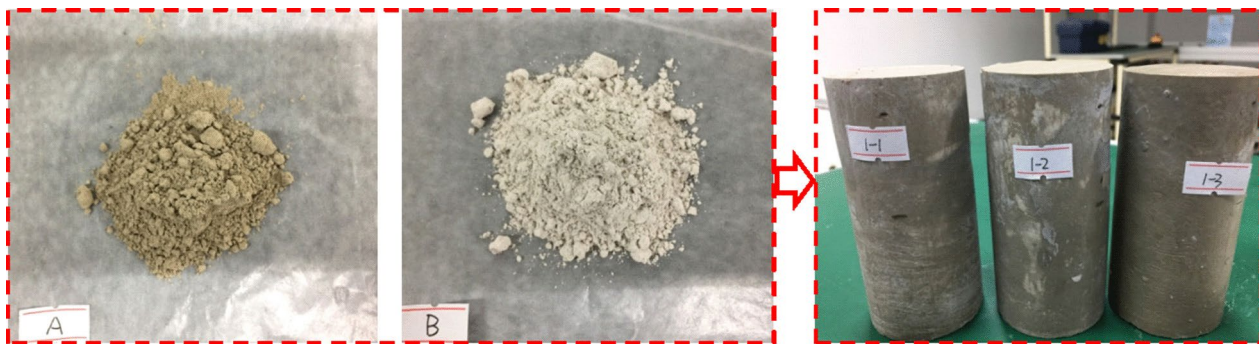
Fig. 5 Preparation process for standard specimens of high-water material

(a) Magnification = 1000×   (b) Magnification = 2000×   (c) Magnification = 3000×
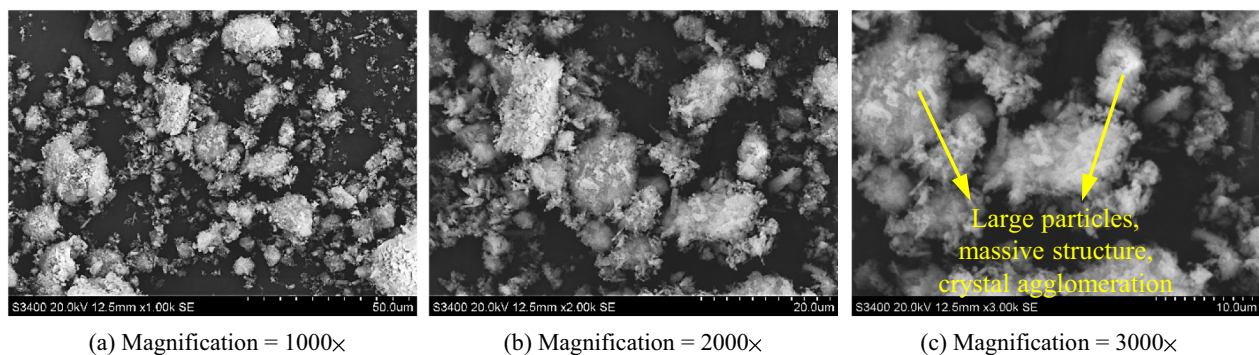
Fig. 6 Morphological characteristics of high-water material with a water-to-cement ratio of 1.6:1

(a) Curing for 1 day

(b) Curing for 3 days

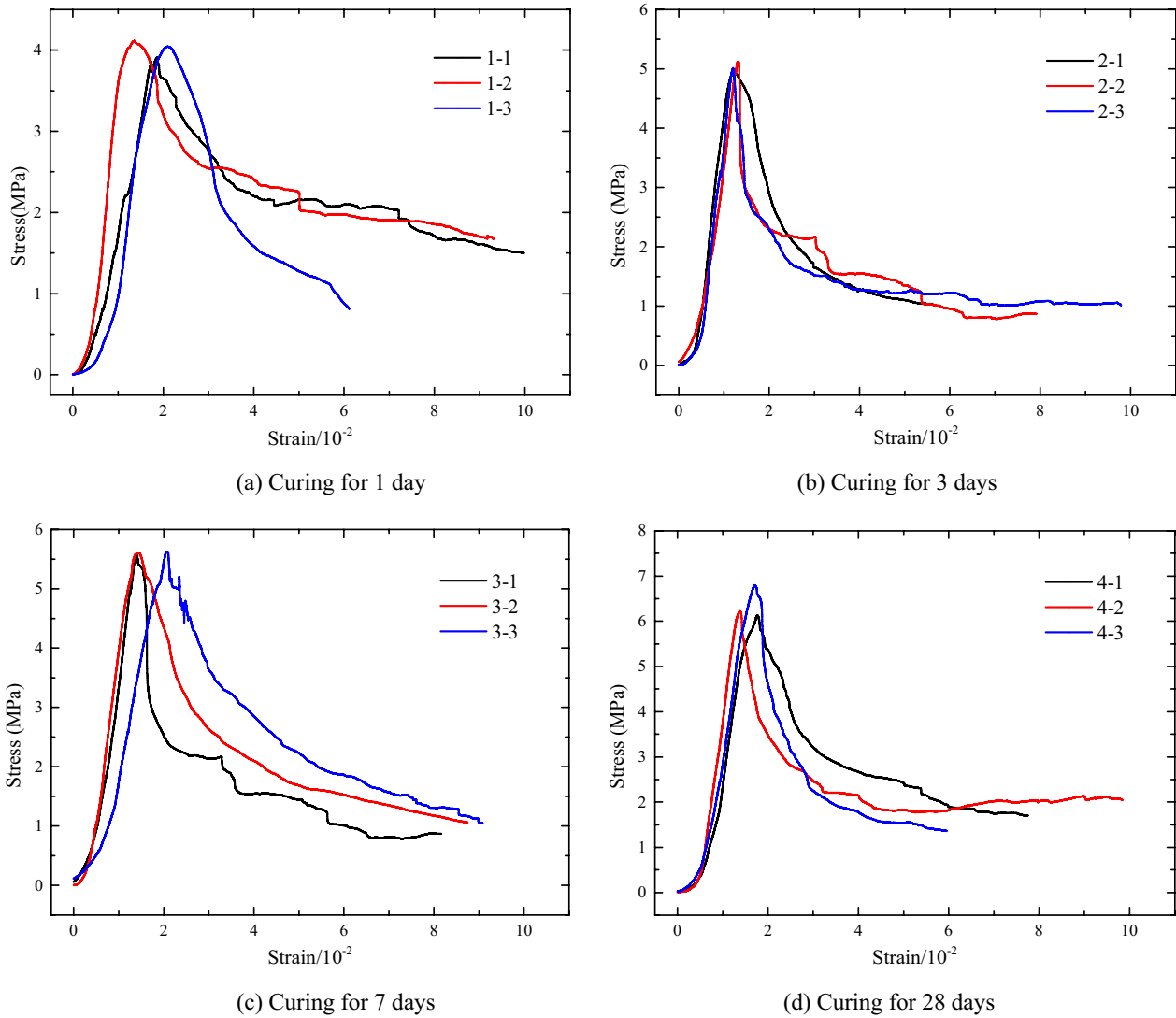(c) Curing for 7 days

(d) Curing for 28 days

Fig. 7 Strength curves of high-water material for different curing ages

3.2 Characteristics of the stress–strain relationship

After preparing $\Phi50\,\text{mm} \times 100$ mm standard cylindrical specimens of high-water material with a water-to-cement ratio of 1.6:1 in the laboratory, we subject the standard specimens with 1-, 3-, 7-, and 28-days curing to uniaxial compressive strength tests. At least three standard specimens are used for each curing age, and the specimen surface is covered after the tests are completed. Standard specimens of high-water material are regularly cured in a constant-temperature (20 ℃) and humid environment (90%), and the uniaxial compressive strength test are conducted for the specimens cured at different ages. The laboratory test results are shown in Fig. 7.

The uniaxial compressive strength tests of high-water material for different curing ages demonstrate the following:
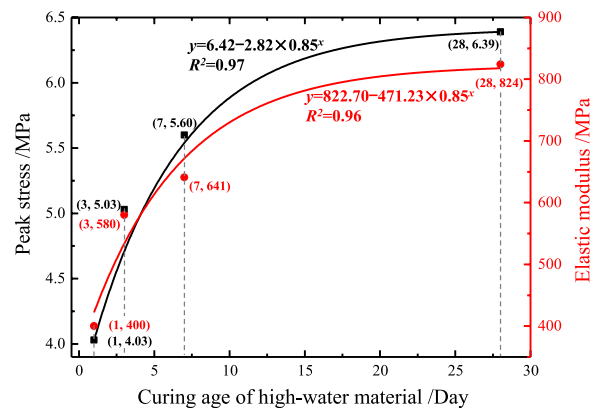

Fig. 8 Curves of peak compressive strength, elastic modulus, and curing age of high-water material
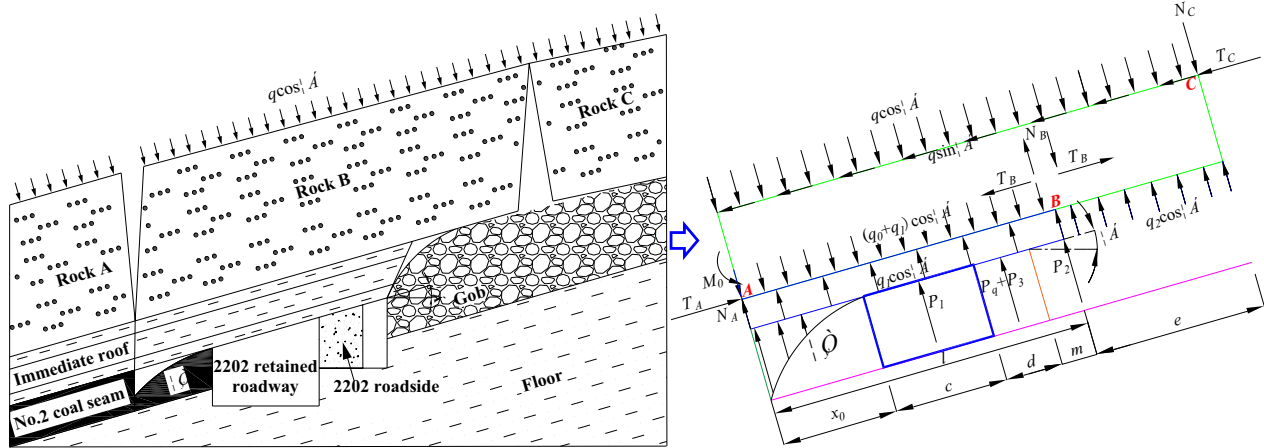
Fig. 9 Mechanical model of GER with double roadways in a gently inclined coal seam

(1) The high-water material has moderate strength and high shrinkage at the initial stage of curing and can adapt to the deformation movement of the overlying main roof in the retained roadway, which plays the role of yielding pressure. (2) The high-water material exhibits obvious plastic characteristics. The stress slowly decreases and tends to a stable value as the strain continued to increase after the peak stress of the high-water material, which means that it still has a certain bearing capacity after plastic failure. This is fundamentally different from brittle materials such as rocks and coal bodies. (3) The peak compressive strength of the high-water material increases significantly with the extension of curing age, while it still exhibits obvious plastic failure characteristics.

Figure 8 shows the average peak compressive strength and elastic modulus of the high-water material for different curing ages. The peak compressive strength is 4.03 MPa after curing for 1 day, and its elastic modulus is 400 MPa. The peak strength and elastic modulus increase rapidly after curing for 3 days, increasing to 5.03 and 580 MPa, respectively. After curing for 7 days, the peak strength and elastic modulus are 5.60 and 641 MPa, respectively. When the curing age increases to 28 days, the peak strength and elastic modulus increase to 6.39 and 824 MPa, respectively. Therefore, the peak compressive strength and elastic modulus of the high-water material both increase with increasing curing age. The strength of the high-water material with a water-to-cement ratio of 1.6:1 reaches 6.39 MPa after curing for 28 days. The elastic modulus of the high-water material within 1-, 3-, 7-, and 28-day curing are 400, 580, 641, and 824 MPa, respectively. The fitting curve for the relationship between the elastic modulus and curing age is determined to be $y = 822.70 - 471.23 \times 0.85^x$, with a goodness of fit, R^2, of 0.96. The relationship between peak stress and curing age is determined to be $y = 6.42 - 2.82 \times 0.85^x$, with a goodness of fit, R^2, of 0.97.

The working face in test mine cuts 5 coal knives every day, with a footage of 0.7 m per knife, with a total footage of 3.5 m per day. The field ground pressure observation results show that the periodic breaking step of the main roof in 2202 working face is 28 m, that is, the main roof breaks periodically after 8 days of mining. It can be seen from Fig. 8 that the strength of high-water material can reach 5.71 MPa after 8 days of curing, that is, 89.36% of the peak compressive strength. Therefore, the high-water material filling body after 8 days of on-site filling is enough to bear the periodic fracture of the main roof and meet the bearing stability requirements of roadside filling body.

In conclusion, the peak strength of roadside high-water material of working face 2202 with a water-to-cement ratio of 1.6:1 can reach 6.39 MPa and the elastic modulus is 824 MPa after curing for 28 days. Therefore, as a new type of filling material, high-water materials have many advantages such as quick solidification, stable performance, obvious plastic characteristics, low cost, and flexibility in adapting to the large deformation of surrounding rock. These materials have been tested and widely used in various coal mines in China.

4 Width determination of GER roadside filling body with double roadways

The simplified mechanical model of the interaction between the roadside support and roof strata is shown in Fig. 9 according to the surrounding rock force of GER and the breaking characteristics of the main roof.

In the above mechanical model of GER with double roadways in a gently inclined coal seam, the formula for the limit equilibrium zone (Huang et al. 2018) on the solid coal side can be expressed as

$$x_0 = \frac{mA}{2\tan\varphi_0} \ln\left[\frac{k\gamma H + \frac{c_0}{\tan\varphi_0}}{\frac{c_0}{\tan\varphi_0} + \frac{p_x}{A}} \right] \tag{1}$$

where x_0 is the limit equilibrium zone on the solid coal side (in meters), m is the mining height ($=1.62$ m), A is the coefficient of lateral pressure ($=1.2$), H is the mining depth ($=670$ m), c_0 is the cohesion force ($=0.9$ MPa), φ_0 is the internal friction angle of the coal ($=32°$), k is the maximum stress concentration factor ($=2.7$), γ is the average weight of overlying rock strata ($=25$ kN/m^3), and p_x is the support strength in solid coal ($=0.28$ MPa). It can be calculated that the limit equilibrium zone x_0 is 5.17 m.

In Fig. 9, the mechanical equilibrium equation for the surrounding rock structure of GER in a gently inclined coal seam is given by

rock B rotates at a certain angle (m); and M_0 is the residual bending moment of the immediate roof (kN m).

The suspension length e of rock B can be calculated using

$$e = \frac{2b}{17} \cdot \frac{b}{L_m} \cdot \sqrt{100 + 102\left(\frac{L_m}{b}\right)^2} - x_0 - c - d \tag{3}$$

where b is the weighting step of the main roof (in meters) and L_m is the length of 2202 working face.

According to Eqs. (2) and (3), combined with the observation results of working face 2202 and its various parameters ($\alpha = 16°$, $x_0 = 5.17$ m, $e = 13.92$ m, $N_C = 0$, $N_A = 0$, $P_1 = P_3 = 360$ kN/m, $P_2 = 180$ kN/m, $q = 903$ kN/m^2, $q_0 = 48.75$ kN/m^2, $q_2 = 14.76$ kN/m^2, $h = 6.02$ m, $c = 4.2$ m, $d = 1.8$ m, $m = 1.0$ m, $l = 12.17$ m, $b = 21$ m, $L_m = 180$ m, $T_C = 2157.60$ kN/m, $\Delta S_B = 0.79$ m, and $M_0 = 0$), the support resistance to be provided for roadside high-water material of GER can be calculated as 10.24 kN/m. It can be seen from the advancement of 2202 working face and the filling process of high-water material that roadside single props need to be safely recovered after 9 days. As can be seen from Fig. 8, the peak compressive strength of roadside high-water material is 5.82 MPa after curing for 9 days. Combined with the calculation formula for the roadside supporting width, the roadside width of the high-water material should be ≥ 1.76 m. The width of roadside high-water material is determined to be 1.8 m and the width-to-height ratio is > 0.6, which satisfies the roadside supporting stability of GER.

$$\begin{cases} q\cos\alpha\frac{(l+e)^2}{2} - q\sin\alpha(l+e)h - N_C(l+e) - q_1\cos\alpha\frac{l^2}{2} - q_2\cos\alpha e\left(l+\frac{e}{2}\right) - T_C(h - \Delta S_B) = 0, \\ q\cos\alpha(l+e) + N_C - q_2\cos\alpha e - N_A - q_1\cos\alpha l = 0, \\ (q_0 + q_1)cos\alpha\frac{l^2}{2} - M_0 - \int_0^{x_0}\sigma_y(x_0 - x)\mathrm{d}x - P_1\left(x_0 + \frac{c}{2}\right) - (P_q + P_3)\left(x_0 + c + \frac{d}{2}\right) - P_2 l = 0, \end{cases} \tag{2}$$

where, σ_y is the support force of coal in the limit equilibrium zone (kN/m^2); P_q is the support resistance of roadside high-water material (kN/m); P_1 is the support resistance of single props in GER (kN/m); P_2 is the support resistance of single props in the outer roadway of GER (kN/m); P_3 is the support resistance of single props on both sides of roadside filling body (kN/m); q_2 is the support force of gangue to rock B (kN/m^2); N_C is the shear of rock C to rock B (kN/m); N_A is the shear of rock A to rock B (kN/m); q is the load of the main roof and overlying soft rock strata (kN/m^2); l is the contact length between the immediate roof and the main roof (m), which can be expressed as $l = x_0 + c + d + m$; e is the suspension length of rock B behind the working face (m) (Chen et al. 2021b, 2022a); q_0 is the weight of the immediate roof (kN/m^2); q_1 is the force of the immediate roof (main roof) to the main roof (immediate roof) (kN/m^2); T_C is the thrust of rock C to rock B (kN/m); h is the thickness of the main roof (m); ΔS_B is the right sinking amount when

5 Stability characteristics of surrounding rock of GER

To study the failure characteristics of surrounding rock of GER, a numerical calculation model is constructed to study the distribution characteristics of the vertical stress and plastic zone when the roadway is undisturbed by working face 2202 and stabilized after mining. This provides a basis for formulating a control scheme for surrounding rock of GER.

5.1 Numerical model

According to the geological conditions of the test mine, FLAC3D simulation software is used to establish a numerical model of GER in 2202 working face, as shown in Fig. 10. In the model, the dip of 2202 working face is taken as 110 m, the advancement is taken as 160 m, the vertical direction of the model is taken as 140 m, and the number of GPS and zones are 821,583 and 787,680, respectively.
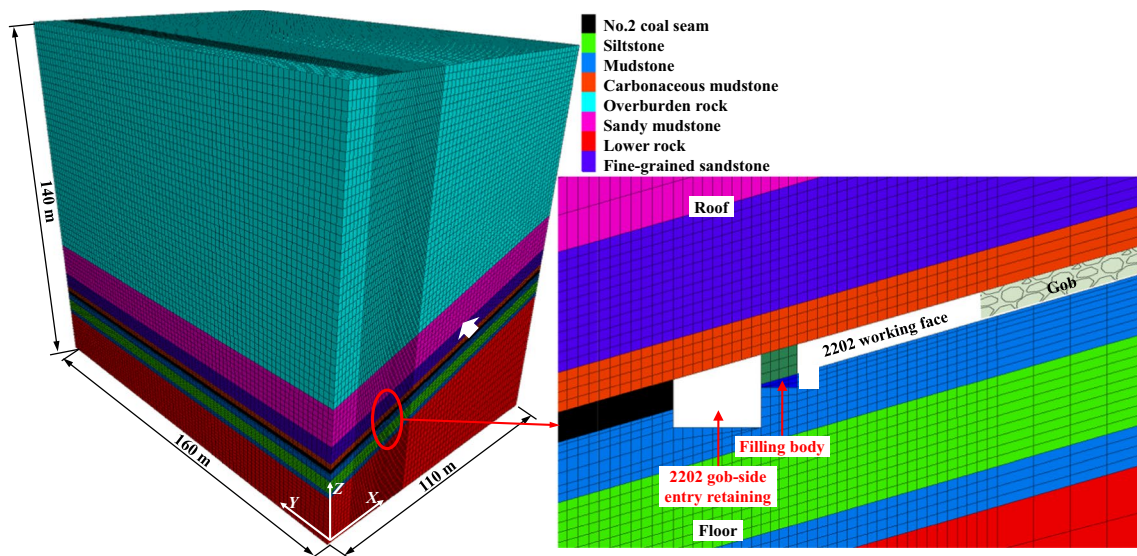
Fig. 10 Numerical model

Table 2 Mechanical parameters of each coal and rock stratum

Lithology	Bulk modulus (GPa)	Shear modulus (GPa)	Cohesion (MPa)	Tensile strength (MPa)	Internal friction angle (°)	Density (g/cm^3)
Sandy mudstone	2.48	2.02	1.97	1.32	24	2.34
Fine-grained sandstone	5.69	2.91	2.32	1.92	29	2.66
Carbonaceous mudstone	2.33	1.91	1.90	1.23	23	2.01
No.2 coal seam	2.28	1.58	1.27	1.13	21	1.35
Mudstone	2.31	1.88	1.86	1.21	22	1.30
Siltstone	4.98	3.54	2.69	2.17	30	2.75

The constitutive relationship of each rock stratum adopted in the model is the Mohr–Coulomb criterion (Yu and Liu 2018; Wang et al. 2020). Roadside high-water material is modeled with a nonlinear strain-softening model, and the goaf is modeled using a double-yield model (Li et al. 2015, 2018). The determination of the mechanical parameters of the coal seams, roof, and floor strata was first made by sampling around the test roadway. The mechanical parameters of each coal and rock stratum required for numerical simulation are calculated using the Hoek–Brown criterion (Medhurst and Brown 1998), as shown in Table 2.

5.1.1 Mechanical parameters of the nonlinear strain-softening model

Strain softening (Zhang et al. 2017) means that the stress quickly decreases to a lower stable value after it reaches the peak as the strain continues to increase while still having a certain bearing capacity. From the uniaxial

Table 3 Parameters of cohesion and friction angle with the change of plastic strain

ε	φ (°)	C (MPa)
0	21.0	0.79
0.017	17.0	0.54
0.021	13.0	0.31
0.026	11.0	0.22

compression stress–strain curves of the high-water material in Fig. 7, we can see that the stress decreases and tends to a stable value as the strain continued to increase after the peak strength of the high-water material is reached. At this time, the high-water material still has a certain bearing capacity. Therefore, the failure process of a high-water material is more in line with the strain-softening model, which is mainly based on the Mohr–Coulomb yield criterion.

The strain-softening parameters ε and φ of roadside high-water material of GER and C of the coal are obtained through laboratory experiments, as listed in Table 3.

Table 4 The cap pressures of the double-yield model

Strain	Stress (MPa)	Strain	Stress (MPa)
0.01	0.14	0.11	3.27
0.02	0.29	0.12	3.88
0.03	0.50	0.13	4.59
0.04	0.71	0.14	5.24
0.05	0.98	0.15	6.74
0.06	1.16	0.16	8.28
0.07	1.43	0.17	10.12
0.08	1.83	0.18	12.97
0.09	2.25	0.19	16.85
0.10	2.69	0.20	22.46

Table 5 Material parameters of the double-yield model

Parameter	D (kg/m^3)	K (GPa)	G (GPa)	φ_m (°)	Dilation (°)
Value	1040	1.17	0.48	18	6

5.1.2 Mechanical parameters of the double-yield model

The roof above the goaf collapsed and is gradually compacted after mining 2202 working face. The modulus increases significantly after compaction. The collapsed goaf not only has to bear part of the roof load but also affects the stress distribution of the floor. Therefore, the double-yield model is used to simulate the strain of the goaf, and the maximum strain and initial modulus of the goaf in FLAC3D are calculated by using the Salamon equation to be 0.23 and 16.26 MPa, respectively. The cap pressures used in the double-yield model are listed in Table 4.

The material parameters of the double-yield model in FLAC3D are listed in Table 5.

### 5.2 Stability analysis of GER with double roadways

FLAC3D numerical calculation software is used to simulate the distribution characteristics of the vertical stress and plastic zone of surrounding rock when the headgate is not disturbed and is affected stably by the mining of 2202 working face (Fig. 11). The vertical stresses of the roof and two sides of the roadway are extracted through a nephogram to analyze the failure characteristics of surrounding rock of GER.

From the distribution curves of vertical stress of the roadway in Figs. 11a, b, it can be seen that the peak stress in solid coal increases from 22.15 MPa when the headgate is not disturbed to 43.85 MPa after mining stability of 2202 working face. The stress concentration factor increases from 1.32 to 2.62 and the peak distance increases from 2.50 to

4.40 m. The peak stress obviously increases and become more deeply affected by the mining disturbance. When the coal on the mining side is not affected by the mining disturbance, the peak stress is approx. 22.49 MPa and the stress concentration factor is 1.34 and the peak distance is 3.0 m, which are slightly larger than that on the solid coal side. After mining of 2202 working face, the roadside high-water material is filled and the stress of the 1.8-m-wide high-water material is low. The vertical stress in the filling body is approximately symmetrical with a peak stress of 5.89 MPa after stability is reached. Figure 8 reveals that the peak compressive strength of the high-water material after curing for 28 days can reach 6.39 MPa with extremely strong plastic characteristics. Therefore, roadside high-water materials can effectively bear the roof load after stability is reached.

As shown in Fig. 11c, the peak zone of the roadway stress is mainly distributed on two sides when the headgate is excavated and not affected by mining of 2202 working face. The peak distances on the solid coal side and mining side are 2.48 and 2.91 m, respectively. The surrounding rock in the shallow roof is in a failure state with a low stress value (Kang 2021; Liu et al. 2020; Wang and Xie 2022; Xie et al. 2022), which is the key control area of surrounding rock of the roadway. Before the mining disturbance of 2202 working face, the plastic zone ranges of the roadway roof, solid coal side, and mining side are 2.94 m, 2.48 m, and 2.83 m, respectively, which are the same as the vertical stress distribution of the roadway approximately. The surrounding rock in the shallow of the roadway undergoes mainly shear and tensile failure. After mining 2202 working face, the peak stress zone of surrounding rock of the retained roadway becomes mainly distributed at 4.77 m from solid coal with a peak stress value of 46.37 MPa, as shown in Fig. 11d. The immediate roof collapses, and the main roof undergoes periodic breakage under mining disturbance (Wang et al. 2019a, b). The roof and floor near the gob side are in a low-stress state on a large scale. Although roadside high-water material is completely in a plastic state, the deformation of the filling body is not large, and it still has a strong bearing capacity (Tan et al. 2015; Yu et al. 2019; Xie et al. 2020). The plastic range on the solid coal side of the retained roadway is 4.26 m, which is approximately consistent with the distribution of the vertical stress.

In summary, the surrounding rock deformation of 2202 GER increases sharply under the mining disturbance of 2202 working face. The peak stress in the solid coal of the roadway increases and moves to a deeper level. The peak stress distance and plastic zone range on the solid coal side are 4.00 and 3.86 m, respectively. The shallow part of the retained roadway roof is in a low-stress state with a large plastic zone, and its goaf roof is in a plastic failure state. The
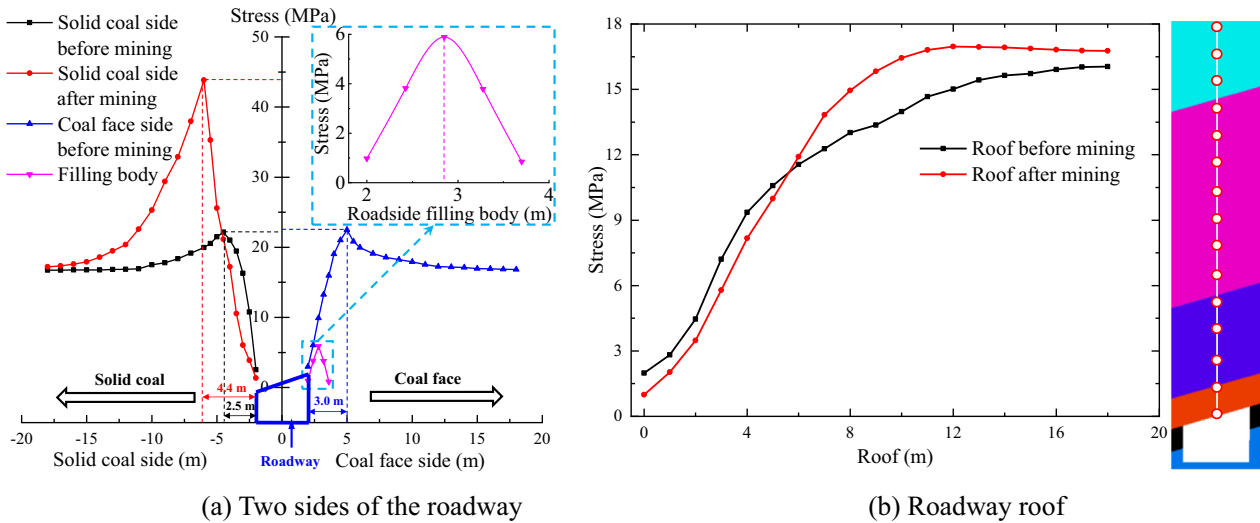
(a) Two sides of the roadway

(b) Roadway roof
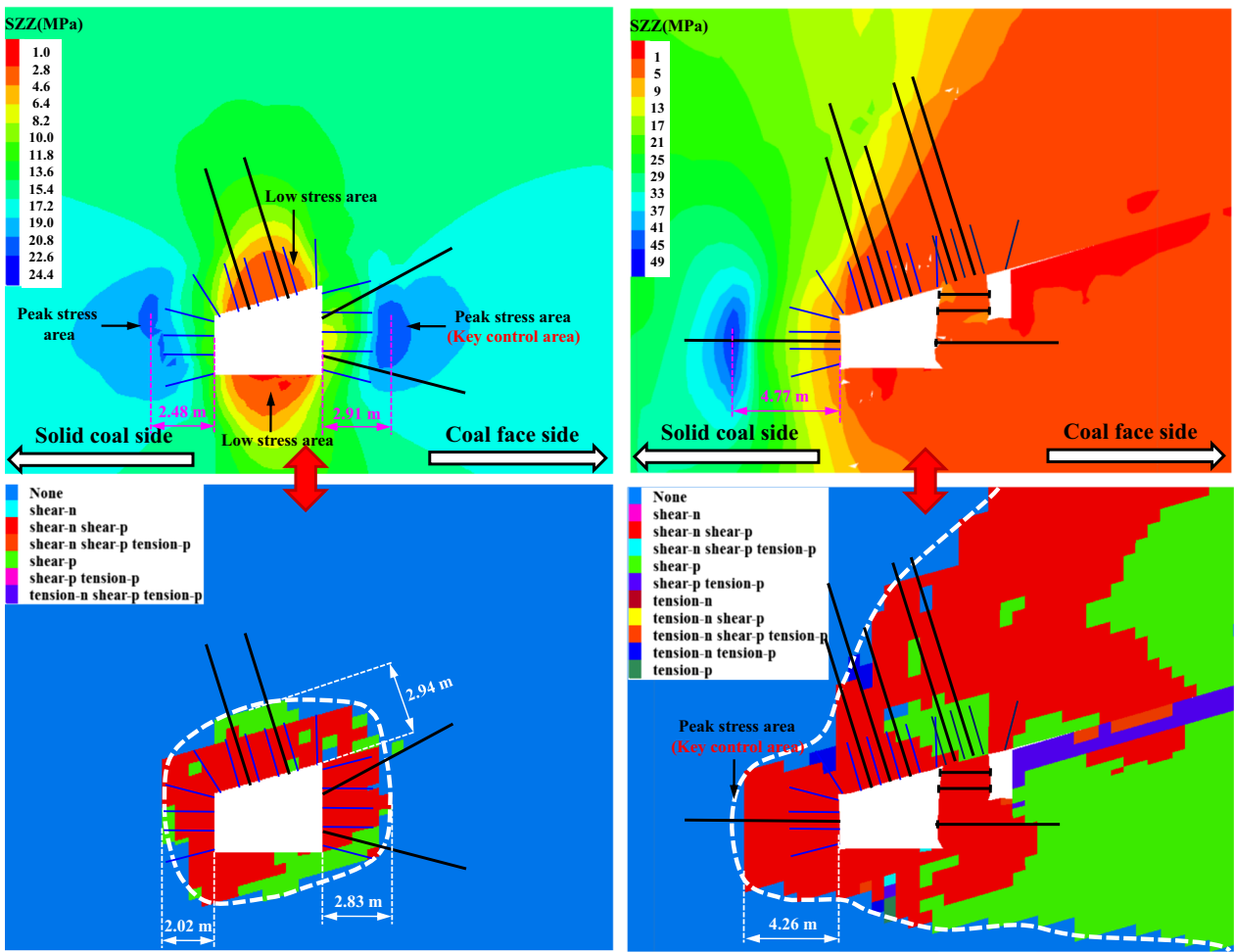
(c) Headgate

(d) Retained roadway

Fig. 11 Vertical stress and plastic zone distribution of roadway surrounding rock

roadside filling body of high-water material is always in a plastic state with a peak stress of 5.89 MPa. Therefore, it is necessary to ensure that the anchor cables pass through the shallow plastically damaged surrounding rock and anchor into the deep stable rock of the retained roadway (Cai 2020; Chen et al. 2022b; Kang et al. 2019; Wang 2020; Yang et al. 2018).

6 Engineering application

Based on the failure range of surrounding rock of GER of 2202 working face in the test mine, a coupling control technology of anchor cables and bolts in the roof and solid coal + single props in the entry-in support and goaf side of the outer roadway + anchor bolts in the roadside high-water material + short anchor cables below the filling body is proposed, and industrial tests are conducted. The reinforcement effects of GER are verified by coupling methods of arranging borehole peeping, observing the convergences, and measuring the load of the filling body.

6.1 GER filling process of roadside high-water material

To ensure that the two parts of the high-water material are not solidified during the transportation process, water is added and the materials are stirred separately using a mixing tank. The dual-liquid filling pump pressurizes the two slurries separately, and the double-pass high-pressure pipeline conveys the slurries into the filling bag, which is then mixed and solidified. The filling procedure for the high-water material of GER in 2202 working faceis shown in Fig. 12.

The anchor bolts are passed through the filling bag and connected to the U-shaped steel, and the single props on the two sides of the roadside filling body are fastened. All the work is checked independently before the pump is started. After the slurries are observed to flow out of the discharge port uniformly, the mixing tube is inserted into the filling bag for formal filling. When the mixture is about to connect the roof,
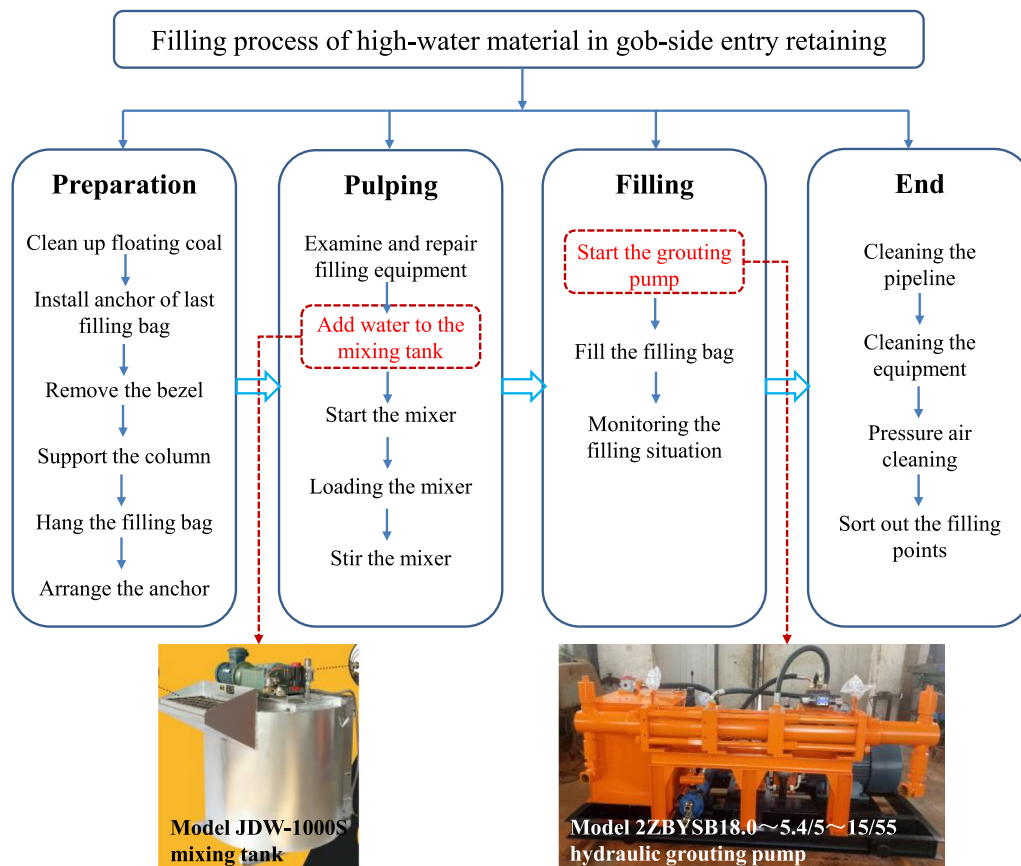

Fig. 12 Filling procedure for high-water material of GER

close observation is made to ensure that the filling bag is tight to the roof without leaving gaps. Once the roof connection is successful, the grouting tube is removed from the filling bag immediately, a signal is sent to stop grouting immediately, and the filling port is firmed with a rope to prevent the slurries from overflowing. At the same time, the staff at the filling station quickly opens the water valve to rinse the mixing pipe to avoid blockage. At the end of the filling work, the pumping station is notified immediately to clean the pipeline using clear water.

6.2 Supporting parameters of surrounding rock of GER

(1) Roof support: A row of $\Phi21.6$ mm $\times 8000$ mm anchor cables are arranged along the roof center of GER, and the row and line spacing is 0.8 m $\times 1.6$ m. The matching square plate is 300 mm $\times 300$ mm $\times 20$ mm with a pre-tightening force of ≥ 250 kN. The row and line spacing of single props is 1400 mm $\times 500$ mm.

(2) Solid coal support: A row of $\Phi21.6$ mm $\times 6000$ mm anchor cables are arranged on the solid coal with a row spacing of 1.6 m. Cables are anchored by CK2335 and Z2360 anchoring agents and connected with steel ladder beams.

(3) Support for expanding the brush section: To ensure the filling construction safety, the filling bag area in front of the support is expanded in advance to a size of 3.6 m $\times 2.8$ m. The $\Phi21.6 \times 8000$ mm anchor cables are arranged perpendicular to the roof with a row and line spacing of 800 mm $\times 1600$ mm. Four $\Phi20$ mm $\times 2000$ mm threaded steel bolts are arranged in each row of the roof. The row spacing of the bolts above the filling body is 800 mm while that of the gob side is 1000 mm. The matching square plate is 150 mm $\times 150$ mm $\times 10$ mm with an anchorage capacity of ≥ 70 kN and a pre-tightening force of ≥ 150 kN.

A metal net of 2.8 m $\times 1.2$ m is laid on the roof of the expanded area. Two rows of cutting props are erected with the articulated roof beam in the filling area near the gob side, and the row spacing is 1.0 m. U-shaped steel and single props are separately supported on both sides of the filling bag with a row spacing of 0.4 m, and the steel is connected by two sections of 1.2-m-long cables to adapt to different heights of the roof. To enhance the stability of the roadside high-water material, $\Phi20$ mm $\times 2200$ mm threaded steel anchor bolts are arranged to punch both sides of the U-shaped steel with a row spacing of 800 mm. The nuts are processed on both ends of the anchor bolts, which are matched with the plate specifications of 150 mm $\times 150$ mm $\times 10$ mm.

There is a 1-m-wide working space between the filling body of GER and the gob. To prevent the gangue

from entering the outer roadway, semicircular timbers are mounted when the single props are erected near the gob side with a spacing of 1 m; these can form a partition wall of the gangue group. The GER supporting scheme with double roadways by filling with a 1.8-m-wide high-water material is shown in Fig. 13.

6.3 Results and analysis of mine pressure observation
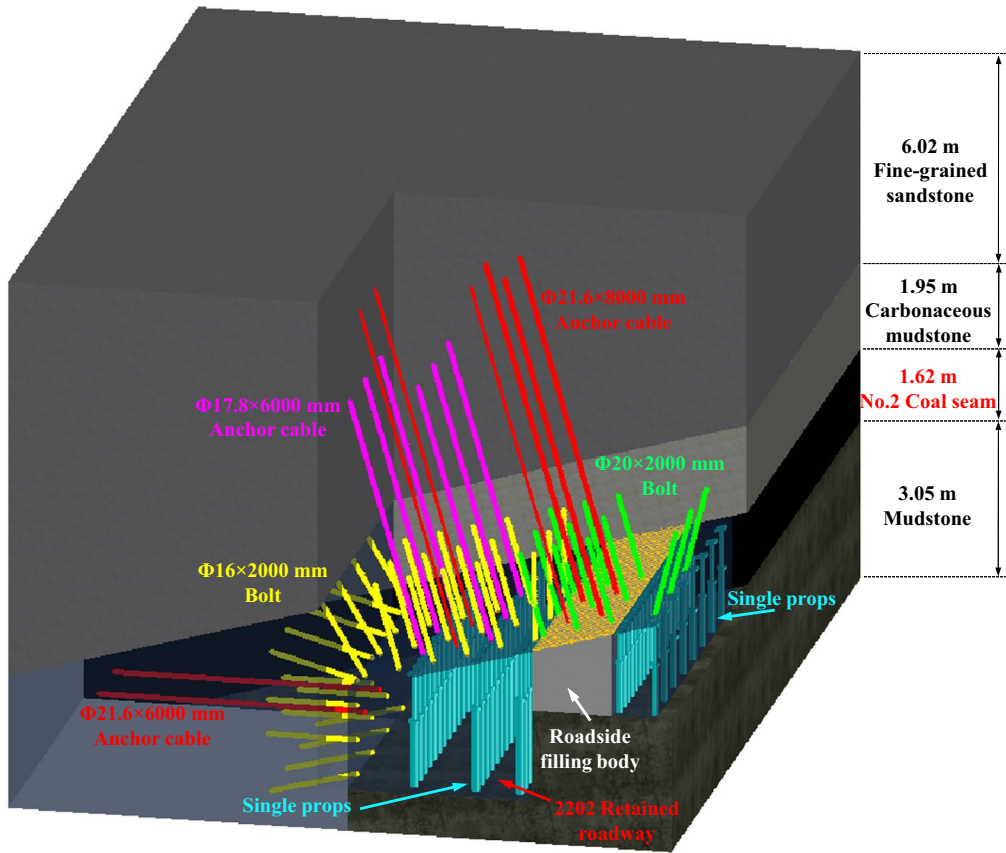
6.3.1 Borehole peeping

The ZKXG100 borehole imaging and trajectory detection instrument (Fig. 14a) is a comprehensive device that is particularly suitable for underground coal mine detection. It can be configured as a drilling peeping device to perform full-hole imaging and recording of various boreholes (Fig. 14b). It is used to observe the geological structural characteristics, such as the occurrence, development, and separation degree of coal seam cracks in the borehole (Wang et al. 2018; Xie et al. 2019). It can also distinguish various geological structures, such as rock masses, coal seams, and gangue.

To verify the control effects of surrounding rock of GER in 2202 working face, borehole imaging and trajectory detection with the ZKXG100 instrument is used to observe the structure. The peeping effects are shown in Fig. 14c. The results show that the coal body is relatively fragmented with many irregular and large fractures within 2.2 m of the initial entrance hole on the solid coal side of the retained roadway. No large fractures are found and the integrity is good at depths of > 2.2 m. Rock mass fissures are well developed in the range of 3.9 m perpendicular to the roadway roof with large fracture apertures. The rock mass integrity is poor and prone to collapse. The number of fractures in the rock mass are significantly reduced, becoming almost zero at depths of > 3.9 m. The loosening damage ranges of the roof angle on the solid coal side and gob side are 1.8 and 5.0 m, respectively. There are many small horizontal, vertical, and irregular cracks and joints distributed in the rock mass, and the rock mass gradually became more complete beyond this range. Therefore, borehole peeping verifies that the long anchor cables have passed through the loosening failure zone in the shallow part of the retained roadway and that the supporting effect of surrounding rock of GER is robust.

6.3.2 Surrounding rock convergences and filling body load

To analyze the failure characteristics of surrounding rock of GER after the coupling control technology is employed, the roof–floor convergence, relative maximum convergence of the two sides, and load of the filling body are used as observation indicators (Fig. 15a). Observation stations are
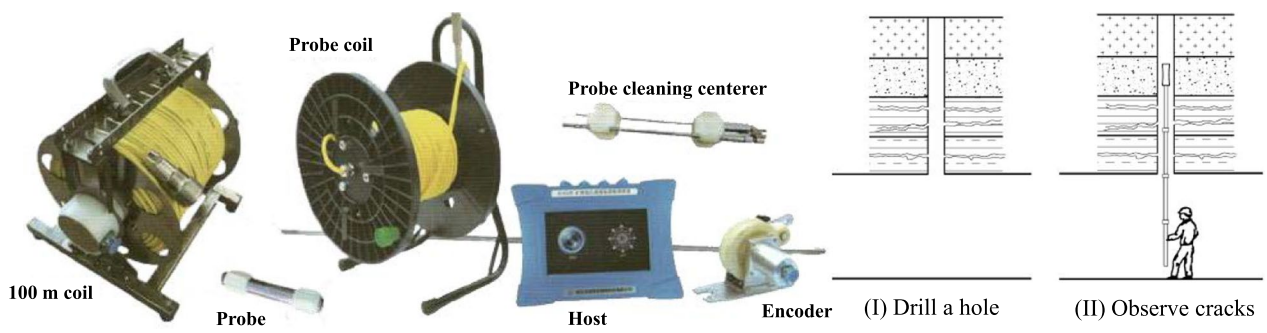
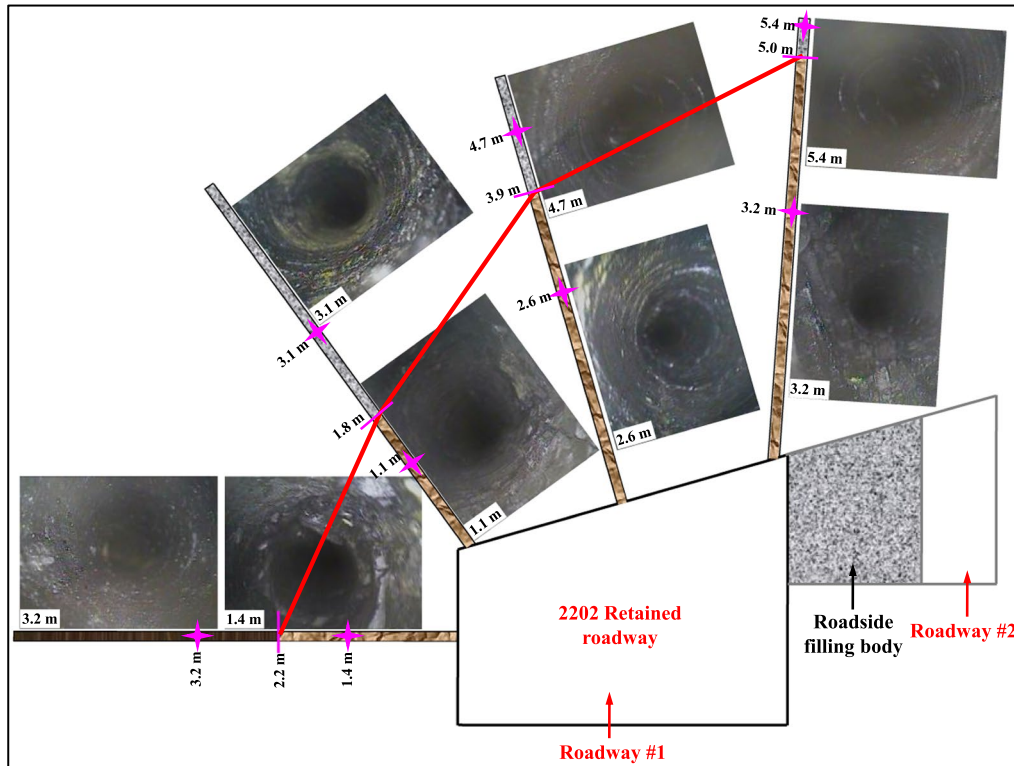(a) Schematic of three-dimensional support
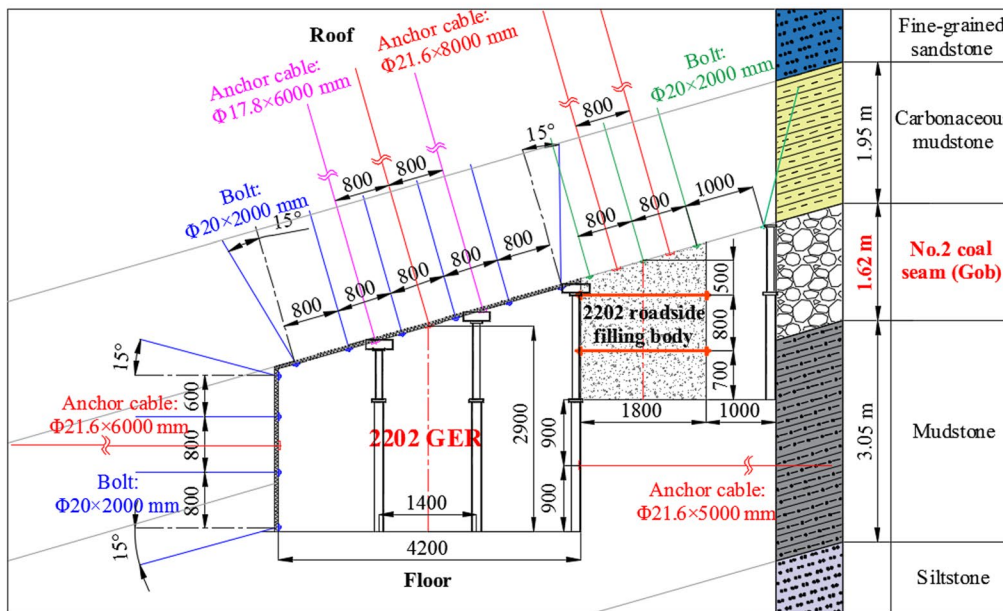
(b) Schematic of the supporting plane

Fig. 13 Supporting scheme of 2202 GER

(a) ZKXG100 borehole imaging and trajectory detection

(b) Sketch map of borehole peeping

(c) Drilling peeping results

Fig. 14 Principles and results of drilling peeping

arranged in the roadway to obtain the deformation of surrounding rock and the load of hydraulic pillows embedded in the filling body, which can provide a basis for evaluating the control effects of surrounding rock. The observation results of the roof–floor convergence, two-side convergence of GER and load of the filling body are shown in Fig. 15b. The roof floor and two sides convergence, and the load of the filling body increase rapidly after the mining of 2202 working face. After the working face advances by 60 m, the relative moving speeds of the two sides and roof floor and the load increasing speed of the roadside filling body gradually slow down. However, the convergences of surrounding rock and the loads of the filling body still exhibited a slow growth trend. After the working face advances 80 m, the convergence of surrounding rock and the load of the filling body of GER don't increase significantly. At this time, the convergences of the two sides and the roof floor are stabilized at 252 and 269 mm, respectively, and the load of the filling body is 5.54 MPa. There is no damage to the supporting system, such as to bolts and anchor cables, and the GER by filling with a 1.8-m-wide high-water material under the mining disturbance meets the actual production needs of the mine. Therefore, the coupling control technology achieves effective control of the deformation of surrounding rock deformation of the retained roadway.
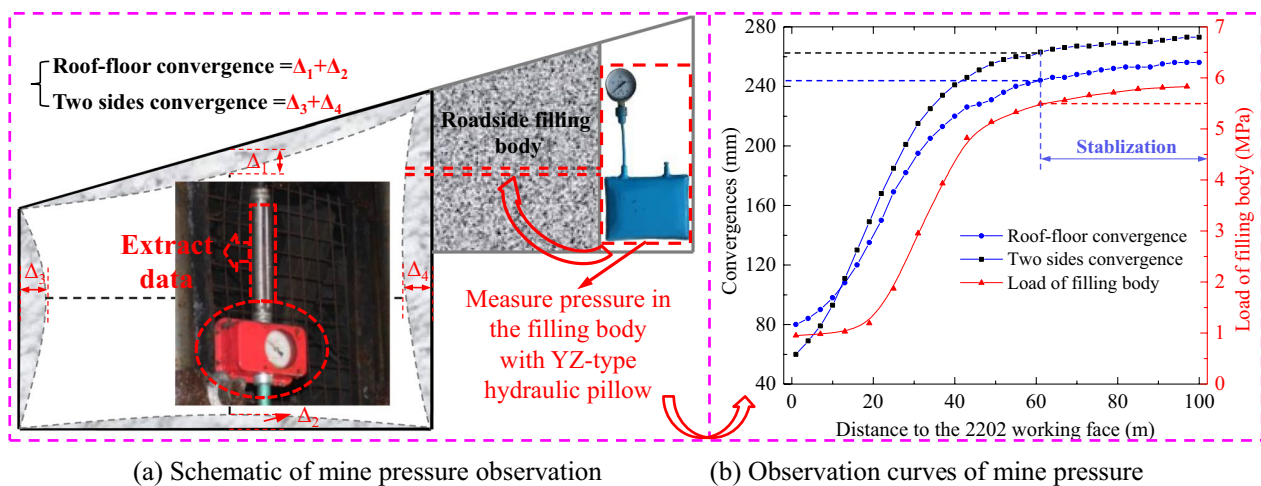
(a) Schematic of mine pressure observation   (b) Observation curves of mine pressure

Fig. 15 Mine pressure curves of 2202 GER

7 Conclusions

(1) The micromorphology of the high-water material is mostly slender needle-like crystals with small crystal diameters, and the inside of the stone body is mainly composed of fine branch-like structures. The high-water material with a water-to-cement ratio of 1.6:1 has a uniaxial compressive strength of 6.39 MPa and an elastic modulus of 824 MPa. The relationship between the elastic modulus and curing age of the high-water material has a fitting curve of $y = 822.70 - 471.23 \times 0.85^x$, with goodness of fit, R^2, of 0.96.

(2) It is determined that the width of the roadside high-water material of GER with double roadways in a gently inclined coal seam is 1.8 m, which is obtained by constructing a mechanical model of GER combined with the peak strength of the high-water material.

(3) The numerical simulation results show that the peak stress in the solid coal of GER increases and moves deeper after stability of the mining disturbance is achieved. The shallow GER roof and the bottom of roadside filling body are in low-stress state, and the ranges of the plastic zone are large. It is concluded that surrounding rock in retained roadway roof, solid coal and filling body floor is unstable, which needs to be strengthened and supported.

(4) Based on the damage range of surrounding rock of GER, a coupling control technology, consisting of anchor cables and bolts in the roof and solid coal + single props in the entry-in support and goaf side of the outer roadway + anchor bolts in the roadside high-water material + short anchor cables below the filling body, is proposed. Based on field application and mine pressure observation, it can be concluded that 2202 GER with double roadways has a good control effect. The results of this study provide a scientific basis for the popularization and application of high-water material for roadside filling of GER in coal mines.

Author contributions All authors read and approved the final manuscript.

Declarations

Ethical approval and informed consent The experiments comply with the current laws of China.

Conflict of interest The authors declare that they have no known competing financial interests or personal relationships that could have appeared to influence the work reported in this paper.

References

Bai JB, Zhou HQ, Hou CJ et al (2004) Development of support technology beside roadway in gob-side entry retaining for next sublevel. J China Univ Min Technol 33(2):59–62

Bai JB, Shen WL, Guo GL et al (2015) Roof deformation, failure characteristics, and preventive techniques of gob-side entry driving heading adjacent to the advancing working face. Rock Mech Rock Eng 48(6):2447–2458. https://doi.org/10.1007/s00603-015-0713-2

Batugin A, Wang Z, Su Z, Sidikovna SS (2021) Combined support mechanism of rock bolts and anchor cables for adjacent roadways in the external staggered split-level panel layout. Int J Coal Sci Technol 8(4):659–673. https://doi.org/10.1007/s40789-020-00399-w

Cai MF (2020) Key theories and technologies for surrounding rock stability and ground control in deep mining. J Min Strata Control Eng 2(3):5–13. https://doi.org/10.13532/j.jmsce.cn10-1638/td.20200506.001

Chang J, He K, Pang D, Li D, Li C, Sun B (2021) Influence of anchorage length and pretension on the working resistance of rock bolt based on its tensile characteristics. Int J Coal Sci Technol 8(6):1384–1399. https://doi.org/10.1007/s40789-021-00459-9

Chen DD, Wang E, Xie SR et al (2020) Roadway surrounding rock under multi-coal-seam mining: deviatoric stress evolution and control technology. Adv Civ Eng. https://doi.org/10.1155/2020/9891825

Chen J, Zhao H, He F, Zhang J, Tao K (2021a) Studying the performance of fully encapsulated rock bolts with modified structural elements. Int J Coal Sci Technol 8(1):64–76. https://doi.org/10.1007/s40789-020-00388-z

Chen DD, Wu YY, Xie SR et al (2021b) Study on the first fracture of the main roof plate structure with one side goaf and elastic-plastic foundation boundary. J Chin Coal Soc 46(10):3090–3105. https://doi.org/10.13225/j.cnki.jccs.2021.0799

Chen DD, Guo FF, Wu YY et al (2022a) Study on the first fracture of the main roof plate structure with the long side goaf and elastic-plastic softening foundation boundary. J Chin Coal Soc 47(4):1473–1489. https://doi.org/10.13225/j.cnki.jccs.2021.1340

Chen DD, Guo FF, Xie SR et al (2022b) Mining-induced failure characteristics and surrounding rock control of gob-side entry driving adjacent to filling working face in the deep coal mine. Energy Sci Eng 1-19. https://doi.org/10.1002/ese3.1214

Feng XW, Zhang N (2015) Position-optimization on retained entry and backfilling wall in gob-side entry retaining techniques. Int J Coal Sci Technol 2(3):186–195. https://doi.org/10.1007/s40789-015-0077-y

He MC, Gao YB, Yang J et al (2017) An innovative approach for gob-side entry retaining in thick coal seam longwall mining. Energies 10(11):1785. https://doi.org/10.3390/en10111785

Huang YL, Zhang JX, Zhang J et al (2011) Technology of gob-side entry retaining on its original position in fully mechanized coalface with solid material backfilling. J Chin Coal Soc 36(10):1624–1628. https://doi.org/10.13225/j.cnki.jccs.2011.10.024

Huang WP, Gao YF, Wen ZJ et al (2015) Technology of gob-side entry retaining using concrete-filled steel tubular column as roadside supporting. J China Univ Min Technol 44(4):604–611. https://doi.org/10.13247/j.cnki.jcumt.000359

Huang BX, Liu JW, Zhang Q (2018) The reasonable breaking location of overhanging hard roof for directional hydraulic fracturing to control strong strata behaviors of gob-side entry. Int J Rock Mech Min Sci 103:1–11. https://doi.org/10.1016/j.ijrmms.2018.01.013

Kang HP (2021) Temporal scale analysis on coal mining and strata control technologies. J Min Strata Control Eng 3(1):5–27 https://doi.org/10.13532/j.jmsce.cn10-1638/td.20200814.001

Kang HP, Niu DL, Zhang Z et al (2010) Deformation characteristics of surrounding rock and supporting technology of gob-side entry retaining in deep coal mine. Chin J Rock Mech Eng 29(10):1977–1987

Kang HP, Xu G, Wang BM et al (2019) Forty years development and prospects of underground coal mining and strata control technologies in China. J Min Strata Control Eng 1(2):7–39. https://doi.org/10.13532/j.jmsce.cn10-1638/td.2019.02.002

Kong DZ, Pu SJ, Cheng ZH et al (2021) Coordinated deformation mechanism of the top coal and filling body of gob-side entry retaining in a fully mechanized caving face. Int J Geomech 21(4):04021030. https://doi.org/10.1061/(ASCE)GM.1943-5622.0001972

Li XL, Liu CW (2018) Mechanical properties and damage constitutive model of high water material at different loading rates. Adv Eng Mater 20(6):1701098. https://doi.org/10.1002/adem.201701098

Li WF, Bai JB, Syd P et al (2015) Numerical modeling for yield pillar design: a case study. Rock Mech Rock Eng 48:305–318. https://doi.org/10.1007/s00603-013-0539-8

Li ZL, He XQ, Dou LM et al (2018) Numerical investigation of load shedding and rockburst reduction effects of top-coal caving mining in thick coal seams. Int J Rock Mech Min Sci 110:266–278. https://doi.org/10.1016/j.ijrmms.2018.08.005

Liu DJ, Zuo JP, Liu HY et al (2020) Development and present situation of support theory and technology in coal mine roadway in China. J Min Sci Technol 5(1):22–33. https://doi.org/10.19606/j.cnki.jmst.2020.01.003

Medhurst TP, Brown ET (1998) A study of the mechanical behaviour of coal for pillar design. Int J Rock Mech Min Sci 35(8):1087–1105

Meng NK, Bai JB, Chen Y et al (2021) Stability analysis of roadside backfill body at gob-side entry retaining under combined static and dynamic loading. Eng Fail Anal 127:105531. https://doi.org/10.1016/j.engfailanal.2021.105531

Orsborn GN, Zantos SG (1988) Corneal desiccation staining with thin high water content contact lenses. CLAO J 14(2):81–85

Park SH, Kim SR, Park M (2019) A comparison of tears volume and lens movement between normal and dry eyes when wearing daily wear soft lenses with high water content. J Korean Ophthalmic Opt Soc 24(4):403–409

Quesada-Kimzey JF, Zuniga P, Gmelch T (2016) Continuous laboratory scale hydrothermal reactor for biomassic materials with high water contents. Abstr Pap Am Chem Soc 251:343

Tan YL, Yu FH, Ning JG (2015) Design and construction of entry retaining wall along a gob side under hard roof stratum. Int J Rock Mech Min Sci 77:115–121. https://doi.org/10.1016/j.ijrmms.2015.03.025

Tang JX, Hu H, Tu XD et al (2010) Experimental on roadside packing gob-side entry retaining for ordinary concrete. J Chin Coal Soc 35(9):1425–1429. https://doi.org/10.13225/j.cnki.jccs.2010.09.015

Tomlinson A, Caroline P (1990) Comparative evaluation of surface deposits on high water content hydrogel contact lens polymers. CLAO J 16(2):121–127

Wang JC (2020) Sustainable coal mining based on mining ground control. J Min Strata Control Eng 1(2):40–47. https://doi.org/10.13532/j.jmsce.cn10-1638/td.2019.02.003

Wang E, Xie SR (2022) Determination of coal pillar width for gob-side entry driving in isolated coal face and its control in deep soft-broken coal seam: a case study. Energy Sci Eng 1-12. https://doi.org/10.1002/ese3.1139

Wang J, Ning J, Jiang L et al (2018) Structural characteristics of strata overlying of a fully mechanized longwall face: a case study. J S Afri Min Metall 118(11):1195–1204. https://doi.org/10.17159/2411-9717/2018/v118n11a10

Wang BN, Dang FN, Wei C et al (2019a) Surrounding rock deformation and stress evolution in pre-driven longwall recovery rooms at the end of mining stage. Int J Coal Sci Technol 6(4):536–546. https://doi.org/10.1007/s40789-019-00277-0

Wang J, Ning JG, Qiu PQ et al (2019b) Microseismic monitoring and its precursory parameter of hard roof collapse in longwall faces: a case study. Geomech Eng 17(4):375–383. https://doi.org/10.12989/gae.2019.17.4.375

Wang Q, Jiang ZH, Jiang B et al (2020) Research on an automatic roadway formation method in deep mining areas by roof cutting with high-strength bolt-grouting. Int J Rock Mech Min Sci 128:104264. https://doi.org/10.1016/j.ijrmms.2020.104264

Wang E, Xie SR, Chen DD et al (2021) Influence of different loading rates on the mechanics and failure characteristics of high-water content material. Geomech Geoengin. https://doi.org/10.1080/17486025.2021.1889688

Wu HK, Liu CW, Zhang Z et al (2020) Time effect of chloride erosion on physical and mechanical properties of high-water-content materials. Adv Mater Sci Eng. https://doi.org/10.1155/2020/2730283

Xia JW, Su Q, Liu DD (2018) Optimal gypsum-lime content of high water material. Mater Lett 215:284–287. https://doi.org/10.1016/j.matlet.2017.12.050

Xie ZZ, Zhang N, Feng XW et al (2019) Investigation on the evolution and control of surrounding rock fracture under different supporting conditions in deep roadway during excavation period. Int J Rock Mech Min Sci 123:104122. https://doi.org/10.1016/j.ijrmms.2019.104122

Xie SR, Wang E, Chen DD et al (2020) Failure analysis and control mechanism of gob-side entry retention with a 1.7-m flexible-formwork concrete wall: a case study. Eng Fail Anal 117:104816. https://doi.org/10.1016/j.engfailanal.2020.104816

Xie SR, Wang E, Chen DD et al (2022) Collaborative control technology of external anchor-internal unloading of surrounding rock in deep large-section coal roadway under strong mining influence. J Chin Coal Soc 47(5):1946–1957. https://doi.org/10.13225/j.cnki.jccs.xr21.1990

Yang HY, Cao SG, Wang SQ et al (2016) Adaptation assessment of gob-side entry retaining based on geological factors. Eng Geol 209:143–151. https://doi.org/10.1016/j.enggeo.2016.05.016

Yang J, Gao YB, Liu SQ et al (2018) Study on failure mechanism and control techniques of the preparation roadway induced by dynamic mining disturbance. J Min Sci Technol 3(5):451–460. https://doi.org/10.19606/j.cnki.jmst.2018.05.005

Yu WJ, Liu FF (2018) Stability of close chambers surrounding rock in deep and comprehensive control technology. Adv Civ Eng. https://doi.org/10.1155/2018/6275941

Yu WJ, Wu GS, An BF et al (2019) Experimental study on the brittle-ductile response of a heterogeneous soft coal rock mass under multi factors coupling. Geofluids. https://doi.org/10.1155/2019/5316149

Zhang GC, He FL, Jia HG et al (2017) Analysis of gate road stability in relation to yield pillar size: a case study. Rock Mech Rock Eng 50:1263–1278. https://doi.org/10.1007/s00603-016-1155-1

Zhang FT, Wang XY, Bai JB et al (2020) Post-peak mechanical characteristics of the high-water material for backfilling the gob-side entry retaining: from experiment to field application. Arab J Geosci 13(11):386. https://doi.org/10.1007/s12517-020-05369-9

Zhou XL, Liu CW, Liu YC et al (2020) Effect of dry-wet cycling on the mechanical properties of high-water materials. Adv Civ Eng. https://doi.org/10.1155/2020/2605751

Publisher's Note Springer Nature remains neutral with regard to jurisdictional claims in published maps and institutional affiliations.